Available online at www.eccomasproceedia.org
Eccomas Proceedia COMPDYN (2019) 2284-2305

ECCOMAS
Proceedia

COMPDYN 2019
7th ECCOMAS Thematic Conference on
Computational Methods in Structural Dynamics and Earthquake Engineering
M. Papadrakakis, M. Fragiadakis (eds.)
Crete, Greece, 24–26 June 2019

A STUDY ON ELASTIC INPUT ENERGY SPECTRA FOR ACTUAL EARTHQUAKE GROUND MOTIONS AT STIFF SOIL SITES

O. Merter[1]
[1] Department of Civil Engineering, Izmir University of Economics
Izmir, 35330, Turkey
e-mail: onur.merter@ieu.edu.tr

Abstract

In energy-based seismic design approach, effect of ground motions on structures is considered as an energy input to structures. The earthquake input energy spectra are created combining the maximum input energies of single-degree-of-freedom (SDOF) systems having a certain damping ratio for different natural vibration periods. The determination of input energy spectra is of great importance for the energy-based seismic design since the total energy input to structural systems can be practically obtained via these graphs. This study presents the investigation of elastic input energy spectra for selected actual earthquake ground motions at stiff soil sites. Accelerogram set is selected from Pacific Earthquake Engineering Research (PEER) database for the specific range of average shear wave velocities in the top thirty meters of soils. Time history analyses are conducted for linear elastic SDOF systems having viscous damping ratio of 5% and energy-time histories are computed. Then the elastic input energy spectra for selected actual earthquake ground motions are obtained. The mean of energy spectra is investigated together with the mean plus one and two standard deviations of the energy spectra. The aim of the present study is to evaluate the earthquake input energy demand spectra of SDOF systems for stiff soil site classes. The results show that the elastic design input energy spectrum can be proposed for selected ground motions at stiff soil sites.

Keywords: Single-Degree-of-Freedom System, Input Energy Spectra, Energy-Based Seismic Design, Earthquake Ground Motion, Soil Site Class.

ISSN:2623-3347
Peer-review under responsibility of the organizing committee of COMPDYN 2019.
doi: 10.7712/120119.7076.18978

1 INTRODUCTION

Earthquake design acceleration spectra are directly used in conventional force-based seismic design and analysis methods to determine the earthquake demand. These spectra are generated to design structures to resist earthquakes considering past seismic activities of a region and they are created for different site conditions, damping ratios, safety levels and earthquake magnitude. Seismic design codes generally define strong ground motion in the form of a response spectrum of acceleration. Equivalent Static Lateral Force method which takes part in many seismic codes such as UBC-97, Eurocode 8, NBCC (2005), IBC (2006), TSDC (2007), ASCE/SEI 7-10 and TBEC (2018) [1-7] directly uses the design acceleration spectra. Response Spectrum Analysis procedure which is a linear-dynamic statistical method computes the maximum seismic response of structures directly considering the design acceleration spectra as in the Equivalent Static Lateral Force method. By brief explanation, the design acceleration spectra are significant graphs which are needed for force-based structural design and therefore they take part in many seismic design codes as standardized graphs [1-7].

In displacement-based seismic design approaches, the structural designer can dimension the structure with required strength and ductility according to a target displacement. The primary design quantity is the target displacement and the inelastic behavior of structures are directly considered in contrast with the force-based procedures [8, 9]. Direct displacement-based design was first introduced by Priestley [10] and after then it received e great deal of attention by countries such as Europe, North America and New Zealand [8, 11, 12]. The fundamental philosophy of this approach is that the structures are designed by using a specified performance level under a specific seismic intensity level. Accordingly, the direct displacement-based design approach is based on the performance-based seismic design which considers direct and indirect displacement of structures to gain the performance objectives [13]. The design displacement response spectra are constructed in direct displacement-based seismic design and then structures are dimensioned to give an effective period. Finally, the total base shear force is determined and it is distributed along the height of the structure [9, 13]. In the course of time, alternative performance-based procedures which use the acceleration response spectra are comprised [9, 14]. The Capacity Spectrum approach, a performance-based seismic analysis technique, establishes the point of structural capacity-earthquake demand balance [14]. Nonlinear static pushover analyses are performed for structures, the pushover (base shear-roof displacement capacity) curves are obtained and they are converted to spectral acceleration and spectral displacement form (ADRS curve). The nonlinear pushover curves become capacity spectra with this conversion process. Then the earthquake demand is represented by acceleration response spectrum and it is reduced with an increasing damping. The intersection of the ADRS curve and the reduced demand spectrum gives the performance point of the structure [15, 16, 17]. Consequently, the design acceleration spectra are directly used to define the demand of earthquake in performance-based seismic design procedures. It can be concluded that the earthquake effect is characterized as a function of the design acceleration spectra both in the force-based and displacement-based (nonlinear static) procedures. In dynamic time history analyses, the design acceleration spectra are indirectly considered [18]. Each ground motion records have different response spectrum depending upon their origin type of earthquakes and local site conditions and target response spectrum is designed in seismic codes considering the large number of ground motions. Therefore, the scaling procedure is applied to ground motions considering the target spectrum in time history analyses and design acceleration spectra have been indirectly used.

Energy concept in seismic design of structures has been widely studied over a half-century period and energy-based methods have always been considered more rational and reliable for the design and assessment of structures under seismic effects when compared to conventional force-based and displacement-based methods [19-21]. In the energy-based methods earthquake effect is considered as an energy input to structures and this energy input expresses the total energy demand of the earthquake. Making a structure safe is considered as a balance of energy dissipation capacity and earthquake energy demand in these approaches. However, an important question of the energy-based seismic design is to determine the energy input to structures with earthquake motion. There have been many previous researches on literature about the energy-based seismic design of structures and seismic input energy. Energy-based earthquake resistant design was first proposed by Housner [22]. Housner studied the seismic energy input to structures using the velocity spectra of elastic systems [22]. Energy-based design parameters were first defined in his researches and these formed a basis for earthquake resistant energy-based design. Some other researchers also made many previous estimations about the input energy concept and they considered the input energy as an effective tool in earthquake-resistant design [19, 23, 24]. Zahrah and Hall [25], Akiyama [26], Kuwamura and Galambos [27], Fajfar et al [28], Uang and Bertero [19] and Manfredi [24] made pioneer studies like Housner [22] about seismic energy concepts and they proposed useful analytical and empirical equations for the seismic input energy. Energy approaches in performance-based seismic design have been studied for nearly two decades by many researchers [29-34]. Practical design procedure based on conventional plastic design concept was proposed by Leelataviwat et al. [32] and the energy-based design base shear was derived considering a predefined yield mechanism. A parametric study to determine the acceptability criteria in structural response parameters corresponding to selected performance levels for specified levels of ground motions was conducted by Akbas and Shen [30]. An energy method for earthquake-resistant design of RC structures was presented in Terapathana's thesis [35]. Nonlinear time history analyses were performed on frame type structures to obtain the required hysteretic energy demands used for the design [35]. Enderami et al. [36] presented a new energy-based approach for predicting seismic demands of steel structures at the near-fault sites. Seismic demands of steel frames were researched by using the concept of dissipated hysteretic energy in their study [36].

The usage of energy spectra is an effective tool in energy-based seismic design methods, such as the use of design acceleration spectra in force-based and displacement-based methods. The obtention of input energy spectra offers an important advantage to determine the energy input to structures with the effect of ground motions. Peak ground acceleration, peak ground velocity, the ratio of peak ground acceleration to peak ground velocity, the duration and predominant periods of ground motions, fault type and mechanism, distance to the fault, the magnitude of ground motions and soil conditions were referred in many previous studies as specific parameters to obtain the seismic input energy spectra [19, 25, 28, 37-44]. Fajfar and Vidic [37], Sucuoglu and Nurtug [38], Decanini and Mollaioli [39], Manfredi [24], Benavent-Climent et al. [40], López-Almansa et al. [41], Dindar et al. [42], Quinde et al. [43], Alici and Sucuoglu [44] and Ozsarac et al. [45] made pioneer and further investigations about the earthquake input energy spectra for both elastic and inelastic systems.

This study presents the development of elastic design input energy spectra using 100 real ground motion records having strike-slip focal mechanism. Accelerograms were obtained from Pacific Earthquake Engineering Research (PEER) database [46]. Selected near-fault and far-fault ground motions are on site class D according to National Earthquake Hazards Reduction Program (NEHRP; Building Seismic Safety Council [47]) site classification. The average shear-wave velocities in the top thirty meters of the soil (V_{S30}) were selected between

the value of 180 m/s and 360 m/s (For Site Class D: Stiff soil with 180 m/s<V_{S30}≤360 m/s [47]). Time history analyses were conducted using selected accelerograms for SDOF systems having damping ratio of 5% and the energy time histories were obtained for different natural vibration periods. The elastic earthquake input energy spectra were created using the data of energy time histories. A computer algorithm was generated by the author to speed up the calculation process and it was used while creating the input energy spectra graphs. The mean elastic input energy spectrum for selected ground motions on the same site class was obtained within the study. The earthquake input energy spectrum graph was also investigated for the mean plus one and two standard deviations of the energy spectra. Then the elastic design input energy spectrum was proposed for selected ground motions and the spectral shape of the design spectrum was obtained. Three main regions of the design spectrum were characterized by equations. The effect of the average shear-wave velocity in the top thirty meters of the soil (V_{S30}) and the effect of the Joyner-Boore distance (R_{JB}) on the elastic design input energy spectrum were also investigated. The variation of the proposed design input energy spectra was obtained for four ranges of V_{S30} (for ranges of 190 m/s<V_{S30}≤235 m/s, 235 m/s<V_{S30}≤280 m/s, 280 m/s<V_{S30}≤325 m/s and 325 m/s<V_{S30}≤370 m/s, respectively) and for four ranges of R_{JB} (for ranges of 0 km<R_{JB}≤46 km, 46 km<R_{JB}≤92 km, 92 km<R_{JB}≤138 km and 138 km<R_{JB}≤184 km, respectively). A comprehensive evaluation was performed in terms of the smoothed mass-normalized earthquake input energy spectra for real ground motions on the stiff soil site. The elastic design input energy spectra were developed for selected accelerograms and the effect of the site class (or V_{S30} velocity) and the effect of the shortest distance from a site to a rupture surface (or R_{JB}) on the design input energy spectra were investigated.

2 ENERGY EQUATION AND BASIC CONCEPT

The energy-balance equation for a SDOF system can be derived by integrating the equation of motion with respect to the relative displacement of the system. A fixed-based SDOF system subjected to a strong ground motion is illustrated in Figure 1. The energy-balance equation of the SDOF system under the effect of strong ground motion can be written as (Uang and Bertero [19]):

$$\int_0^{u(t)} m\cdot\ddot{u}\,du + \int_0^{u(t)} c\cdot\dot{u}\,du + \int_0^{u(t)} f_s(u)\,du = -\int_0^{u(t)} m\cdot\ddot{u}_g(t)\,du \tag{1}$$

where u is the relative displacement of the SDOF system with respect to the ground, $\dot{u}$ is the relative velocity, $\ddot{u}$ is the relative acceleration, m is the total mass, c is the damping coefficient, $f_s(u)$ is the resisting force and is the strong ground acceleration. In Figure 1, u_t shows the total displacement of the structure under the effect of strong ground motion and it is equal to the sum of relative displacement and displacement of the ground ($u_t=u+u_g$). k is the stiffness of the SDOF system and the resisting force $f_s(u)$ is equal to $k.u$ for linear elastic systems. Equation (1) may be restated in general types of energy components as below:

$$E_K+E_\xi+E_S=E_I \tag{2}$$

On the left-hand side of Equation (1) the first integral term is the kinetic energy, the second integral term is the damping energy and the last integral term represents the total absorbed energy. In Equation (2), in which the symbolic expressions of the energy-balance equation are involved, these integrals are written as in the form of representative energy terms. E_K represents the relative kinetic energy, E_ξ represents the damping energy, E_S represents the total absorbed energy and E_I stands for the total input energy.

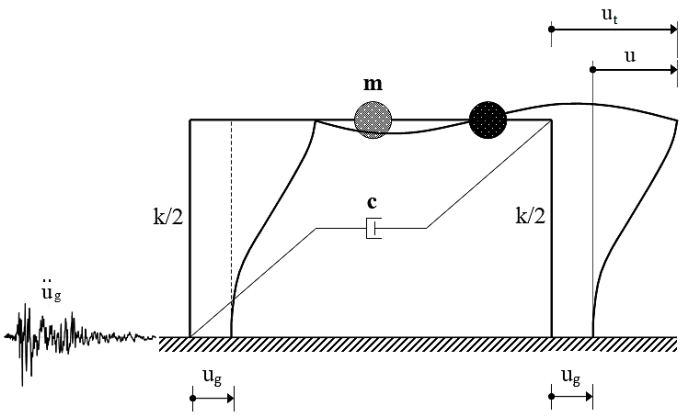

Figure 1: Fixed-based SDOF system subjected to a strong ground motion.

The energy E_S is composed of two parts as elastic strain energy (E_{Se}), and hysteretic (irrecoverable plastic) energy (E_H) which is the main energy component in nonlinear behavior. Equation (2) may be rewritten as:

$$E_K+E_\xi+\{E_{Se}+E_H\}=E_I \tag{3}$$

The energy-balance equation for a SDOF structure based on relative motion can be rewritten in terms of time integral writing a derivative equality for du ($du=\dot{u}\,dt$) as ([19]):

$$\int_0^t m\cdot\ddot{u}\cdot\dot{u}\,dt+\int_0^t c\cdot\dot{u}\cdot\dot{u}\,dt+\int_0^t f_s(u)\cdot\dot{u}\,dt=-\int_0^t m\cdot\ddot{u}_g(t)\cdot\dot{u}\,dt \tag{4}$$

The energy input to SDOF structures can be computed by using the right-hand side term of Equation (4). This is the total input energy of SDOF systems under the effect of strong ground motion. The energy E_I can be rewritten independent of the mass (per unit mass) as:

$$\frac{E_I}{m}=-\int_0^t \ddot{u}_g(t)\cdot\dot{u}\,dt \tag{5}$$

The representative energy-time history graph of an inelastic SDOF structure under a strong ground motion effect is given in Figure 2. The sum of the elastic strain energy (E_{Se}), kinetic energy (E_K), damping energy (E_ξ) and hysteretic energy (E_H) is equal to the total input energy (E_I) as can be seen from the figure.

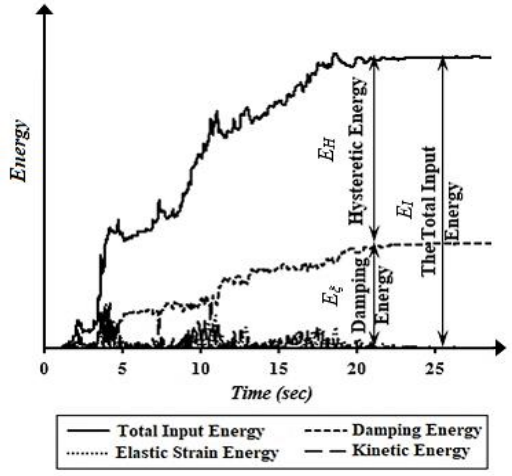

Figure 2: The representative energy-time history graph of an inelastic SDOF system.

The substantial components of the earthquake input energy are the damping energy (E_ξ), and the hysteretic energy (E_H) which contributes the most to structural damage. The input energy E_I generally tends to be constant towards the end of the earthquake duration.

3 INPUT ENERGY SPECTRA

In the field of energy-based earthquake-resistant design of structures, the energy demand of an earthquake should be less than (or, in limit, should be equal to) the energy dissipation capacities possessed by the structure (Decanini and Mollaioli [39]). It is of utmost importance for structural and earthquake engineers that the seismic input energy demand transmitted to structures is computed exactly. However, this process involves detailed dynamic analyses and therefore many researchers have sought to obtain practical ways for computation of the input energy. In literature, many approximate formulas have been proposed for obtention of the maximum seismic input energy [19, 22, 24-28]. Moreover, the seismic input energy spectra have been created for a specific strong ground motion and the input energy values of both elastic and inelastic systems have been obtained practically via these graphs [24, 37-45]. In brief definition, the seismic input energy spectra are the graphs which combine the maximum energy input values corresponds to different natural vibration periods of SDOF systems. There are many factors (such as earthquake magnitude, closest distance from the seismic source, soil type, focal mechanism, damping ratio, type of hysteresis for the inelastic spectra, and etc.) which have an impact on the seismic input energy spectra [39, 42, 43].

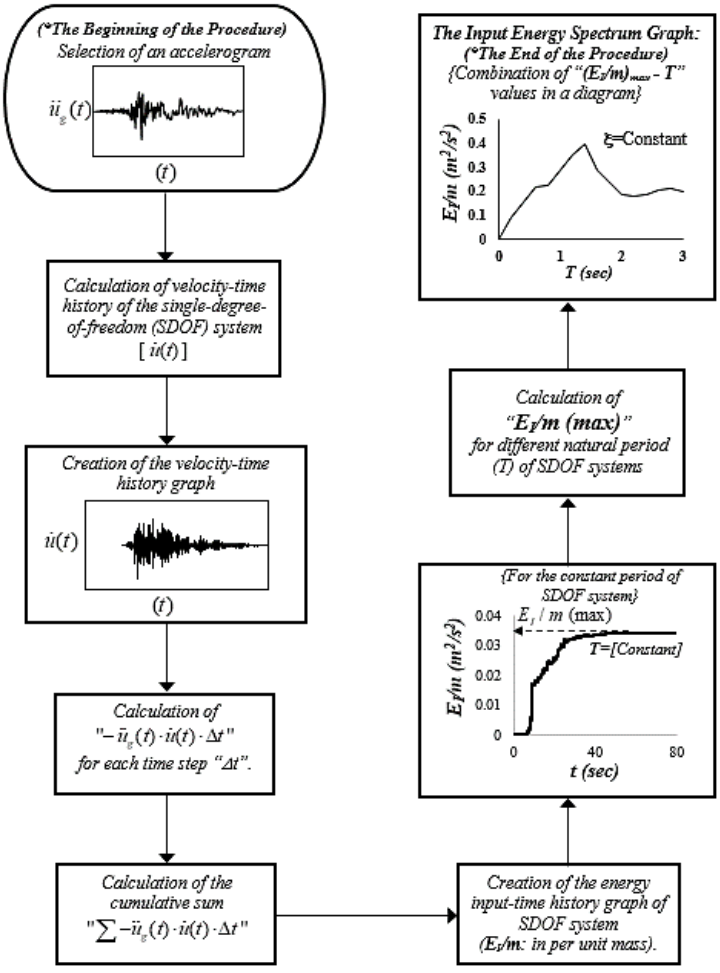

Figure 3: The flowchart to obtain the input energy spectra graphs.

The flowchart to obtain the input energy spectra is presented in Figure 3. The procedure begins with the selection of an accelerogram and continues with the calculation of velocity-time history ($\dot{u}(t)-t$) relation for SDOF structure. After computing the energy input-time history graph in per unit mass, the maximum input energy value ($(E_I/m)_{max}$) can be readily determined for the constant period of structure. When adequate number of "$(E_I/m)_{max}$-T" points are obtained, the combination of these values in a diagram gives the input energy spectra graph. If the SDOF structure is linearly elastic the input energy spectra may be called as the elastic input energy spectra, and if the nonlinear behavior of the structure is taken into consideration in dynamic analyses the input energy spectra may be called as the inelastic input energy spectra.

4 STRONG GROUND MOTION RECORDS

100 real ground motion records having strike-slip focal mechanism have been selected within the study. The average shear-wave velocities in the top thirty meters of the soil (V_{S30}) have been selected between the value of 180 m/s and 360 m/s. Soil class is D (stiff soil with 180 m/s<V_{S30}≤360 m/s) according to National Earthquake Hazards Reduction (NEHRP) Program site classification [47]. Moment magnitudes (M_w) of earthquakes are between 6.0 and 7.5. Joyner-Boore distances (R_{JB}) are between 0 km and 175 km and values of closest distance to rupture surface ($R_{rupture}$) are between 0.34 km and 175 km. The peak ground accelerations (*PGA*) are between the values of 0.011g and 0.777g. All of the selected accelerograms in the study are obtained from the database of Pacific Earthquake Engineering Research Center, PEER [46].

The selection of accelerograms is an important issue among structural and earthquake engineers to assess the structural performance. Real earthquake records may be selected in accordance with the specific characteristics of the ground motion [48, 49]. The selection is generally executed considering an elastic response spectrum, an earthquake scenario or seismological parameters etc. Many seismic codes present criteria compatible with response spectrum for the appropriate ground motion selection. Magnitude of earthquake is another important parameter for the ground motion selection because it influences the frequency content of the motion, so the appropriate magnitudes should be selected in an earthquake data set [48]. Strong ground motion parameters such as peak ground acceleration (*PGA*), peak ground velocity (*PGV*) and peak ground displacement (*PGD*) are the other parameters that should be taken into consideration in the selection of accelerogram with fault-site distances and soil site conditions [48-50]. If the selected accelerograms will be used to perform dynamic time history analyses, they should be scaled according to the suitable design acceleration spectrum using an appropriate scaling method (to match the spectra) [48-50].

In this study, the elastic earthquake input energy spectra for selected real accelerograms have been investigated and the elastic design input energy spectra has been proposed. The effect of the average shear-wave velocity in the top thirty meters of the soil (V_{S30}) and the effect of the Joyner-Boore distance (R_{JB}) on the design input energy spectra have been studied. The primary aim of the study is only to propose the elastic design input energy spectra for real and unscaled ground motions on the specific soil site. The analyses were carried out by using unscaled ground motion data, because the proposed energy spectra would not be used in any assessment of structural performance (or analysis). In the selected accelerogram set, there are some records having the source-to-site distance is less than 15 km ($R_{rupture}$<15 km) but most part of the set have the source-to-site distance value greater than 40 km ($R_{rupture}$<40 km: far-fault earthquake). In other words, the near fault earthquakes were not sorted out from the set, because the aim is not to obtain the near fault effects to the energy spectra but the aim is only

to investigate the effect of V_{S30} (soil class) and R_{JB}. The effects of near faults on elastic or inelastic energy spectra can be investigated in another studies.

Selected earthquake records are given in Table 1, Table 2 and Table 3, in three parts. Earthquakes between the number of 1 and 34 are presented in Table 1, earthquakes 35-67 are presented in Table 2 and earthquakes 68-100 are presented in Table 3. I_A is the Arias Intensity, as defined by Arias [51], and it is proportional to the square of the ground acceleration integrated over time. Arias Intensity may be written as:

$$I_A = \frac{\pi}{2g} \cdot \int_0^{t_d} a^2(t)\, dt \tag{6}$$

where $a(t)$ is the strong ground acceleration, t_d is the total earthquake duration, g is the acceleration of gravity and I_A is the Arias Intensity in m/s unit.

Event Name (*1)	***Station***	***Year***	M_w	I_A ***(m/s)***	R_{JB} ***(km)***	V_{S30} ***(m/s)***	***PGA (g)***	***PGV (cm/s)***	***PGD (cm)***
Big Bear	San B. - E & Hospitality	1992	6.46	0.3	34.98	296.97	0.101	11.90	3.35
Borrego Mtn	El Centro Array 9#	1968	6.63	0.2	45.12	213.44	0.133	26.70	14.60
Erzincan	Erzincan	1992	6.69	1.8	0	352.05	0.496	78.10	28.01
Kocaeli	Duzce	1999	7.51	1.3	13.6	281.86	0.312	58.80	44.11
Landers	Yermo Fire	1992	7.3	0.71	23.62	353.6	0.152	29.70	24.69
Nicaragua-01	Managua ESSO	1972	6.24	2	3.51	288.77	0.337	30.70	6.16
Trinidad	Rio Dell Overpass	1980	7.2	0.4	76.06	311.75	0.151	8.86	3.60
Imp. Valley-02	El Centro Array #9	1940	6.95	1.6	6.09	213.44	0.211	31.32	24.16
Northw. Calif-02	Ferndale City Hall	1941	6.6	0	91.15	219.31	0.040	6.83	4.48
Northern Calif-01	Ferndale City Hall	1941	6.4	0.1	44.52	219.31	0.122	13.53	5.30
Northern Calif-03	Ferndale City Hall	1954	6.5	0.5	26.72	219.31	0.203	52.40	39.40
El Alamo	El Centro Array #9	1956	6.8	0.1	121	213.44	0.050	14.16	16.34
Parkfield	Cholame – Sh. Array #5	1966	6.19	0.9	9.58	289.56	0.368	22.51	4.56
Parkfield	Cholame – Sh. Array #8	1966	6.19	0.4	12.9	256.82	0.272	11.36	3.81
Imp. Valley-06	Aeropuerto Mexicali	1979	6.53	1.2	0	259.86	0.271	24.19	3.71
Imp. Valley-06	Bonds Corner	1979	6.53	6.1	0.44	223.03	0.777	44.93	15.10
Imp. Valley-06	Calexico Fire Station	1979	6.53	0.9	10.45	231.23	0.203	18.65	15.88
Imp. Valley-06	Calipatria Fire Station	1979	6.53	0.1	23.17	205.78	0.078	27.36	27.41
Imp. Valley-06	Chihuahua	1979	6.53	1.2	7.29	242.05	0.254	29.89	7.65
Imp. Valley-06	Coachella Canal #4	1979	6.53	0.2	49.1	336.49	0.128	32.00	13.03
Imp. Valley-06	Compuertas	1979	6.53	0.4	13.52	259.86	0.147	9.32	2.89
Imp. Valley-06	Delta	1979	6.53	3.3	22.03	242.05	0.350	32.99	20.17
Imp. Valley-06	El Centro Array #1	1979	6.53	0.3	19.76	237.33	0.136	10.97	7.10
Imp. Valley-06	El Centro Array #11	1979	6.53	2	12.56	196.25	0.379	44.60	21.32
Imp. Valley-06	El Centro Array #12	1979	6.53	0.4	17.94	196.88	0.118	45.98	53.39
Imp. Valley-06	El Centro Array #13	1979	6.53	0.3	21.98	249.92	0.139	13.65	7.73
Imp. Valley-06	El Centro Array #8	1979	6.53	1.6	3.86	206.08	0.466	52.07	41.12
Imp. Valley-06	Niland Fire Station	1979	6.53	0.2	35.64	212	0.070	8.57	5.17
Imp. Valley-06	Parachute Test Site	1979	6.53	0.2	12.69	348.69	0.206	17.71	12.19
Imp. Valley-06	Plaster City	1979	6.53	0.1	30.33	316.64	0.058	5.85	2.49
Imp. Valley-06	Victoria	1979	6.53	0.3	31.92	242.05	0.168	8.84	1.93
Imp. Valley-06	Westmorland Fire Sta	1979	6.53	0.1	14.75	193.67	0.111	22.60	11.25
Victoria_ Mexico	Chihuahua	1980	6.33	0.4	18.53	242.05	0.097	18.49	18.41
Victoria_ Mexico	SAHOP Casa Flores	1980	6.33	0.1	39.1	259.59	0.069	8.94	2.18

Table 1: Selected earthquake records [Part I: EQ 1-34], [46].

Moment magnitudes (M_w) of selected earthquakes can be seen from Figure 4. Moment magnitude of the large majority of records is M_w=7.28 (41 earthquake records). In Figure 5, the average shear-wave velocities (V_{S30} values) in the top thirty meters of the soil for 100 selected earthquakes are given (180 m/s<V_{S30}≤360 m/s, Soil Class D (NEHRP, [47])). Figure 6a shows the moment magnitude (M_w) versus distance (R_{JB}) distribution of selected earthquake data set and Figure 6b gives the moment magnitude (M_w) versus *PGA* (g) distribution of the same data set.

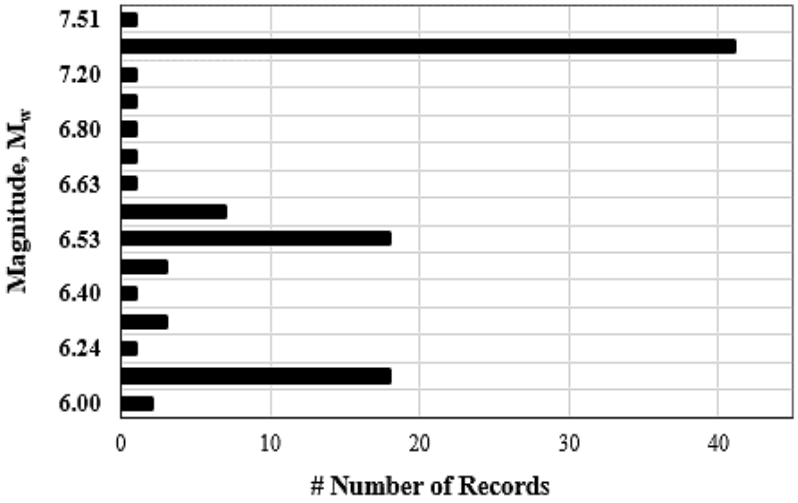

Figure 4: Number of records corresponding to moment magnitudes (M_w).

*Event Name (*2)*	*Station*	*Year*	M_w	I_A *(m/s)*	R_{JB} *(km)*	V_{S30} *(m/s)*	*PGA (g)*	*PGV (cm/s)*	*PGD (cm)*
Victoria	Victoria Hos. Sotano	1980	6.33	0	6.07	242.05	0.033	5.55	1.51
Morgan Hill	APEEL 1E – Hayward	1984	6.19	0	51.68	219.8	0.027	4.59	2.86
Morgan Hill	Agnews State Hos.	1984	6.19	0.1	24.48	239.69	0.032	5.63	2.19
Morgan Hill	Capitola	1984	6.19	0.2	39.08	288.62	0.142	8.29	1.67
Morgan Hill	Gilroy Array #2	1984	6.19	0.2	13.68	270.84	0.213	12.74	2.48
Morgan Hill	Gilroy Array #3	1984	6.19	0.3	13.01	349.85	0.201	13.30	3.66
Morgan Hill	Gilroy Array #4	1984	6.19	0.8	11.53	221.78	0.349	17.30	3.31
Morgan Hill	Gilroy Array #7	1984	6.19	0.3	12.06	333.85	0.114	5.55	1.17
Morgan Hill	Halls Valley	1984	6.19	0.9	3.45	281.61	0.312	39.32	7.02
Morgan Hill	Hollister City Hall	1984	6.19	0.2	30.76	198.77	0.071	9.91	5.27
Morgan Hill	Hollister Diff. Array #3	1984	6.19	0.1	26.42	215.54	0.079	7.05	1.41
Morgan Hill	Los Banos	1984	6.19	0	63.16	262.05	0.062	9.16	2.27
Morgan Hill	SF Intern. Airport	1984	6.19	0	70.93	190.14	0.048	2.91	0.50
Morgan Hill	San Juan B._ 24 Polk St	1984	6.19	0	27.15	335.5	0.036	4.70	1.81
Chalf. Vall.-02	Bishop–LADWP South	1986	6.19	0.5	14.38	303.47	0.176	19.53	7.09
Chalf. Vall.-02	McGee Creek - Surface	1986	6.19	0.1	28.2	359.23	0.084	2.33	0.10
Chalf. Vall.-02	Zack Brothers Ranch	1986	6.19	2	6.44	316.19	0.401	44.72	8.57
Supers. Hills-02	Brawley Airport	1987	6.54	0.3	17.03	208.71	0.111	15.99	6.90
Supers. Hills-02	Calipatria Fire Station	1987	6.54	0.5	27	205.78	0.259	14.97	3.35
Supers. Hills-02	El Centro Imp.Co.Cent	1987	6.54	1.1	18.2	192.05	0.259	41.78	21.85
Supers. Hills-02	Plaster City	1987	6.54	0.6	22.25	316.64	0.200	21.59	5.09
Supers. Hills-02	Poe Road (temp)	1987	6.54	2.1	11.16	316.64	0.286	29.01	11.36
Supers. Hills-02	Salton Sea Wildlife R.	1987	6.54	0.4	25.88	191.14	0.140	18.11	4.31
Supers. Hills-02	Westmorland Fire Sta	1987	6.54	1.2	13.03	193.67	0.211	32.32	22.31
Landers	Anaheim – W Ball Rd	1992	7.28	0.1	144.9	269.29	0.038	12.47	8.99
Landers	Arcadia – Arcadia Av	1992	7.28	0	137.25	330.5	0.028	9.24	6.62
Landers	Baker Fire Station	1992	7.28	0.3	87.94	324.62	0.106	10.97	7.96
Landers	Bell Gardens–Jaboneria	1992	7.28	0.1	154.26	267.13	0.045	13.20	16.96
Landers	Boron Fire Station	1992	7.28	0.2	89.69	291.03	0.090	9.55	3.39
Landers	Brea - S Flower Av	1992	7.28	0.1	137.44	322.75	0.044	15.10	11.91
Landers	Buena Park – La Palma	1992	7.28	0.1	150.09	270.96	0.043	13.29	19.76
Landers	Burbank – N B. Vista	1992	7.28	0.2	157.94	320.57	0.065	13.41	7.97
Landers	Compton – Castl. St	1992	7.28	0.2	161.23	266.9	0.066	13.22	11.82

Table 2: Selected earthquake records [Part II: EQ 35-67], [46].

Figure 7 shows the distribution of strong motion data in terms of Joyner-Boore distance (R_{JB}). *PGA*-R_{JB} relation is given in Figure 7a and *PGV*-R_{JB} relation is given in Figure 7b. Distance variables are expressed in logarithmic form.

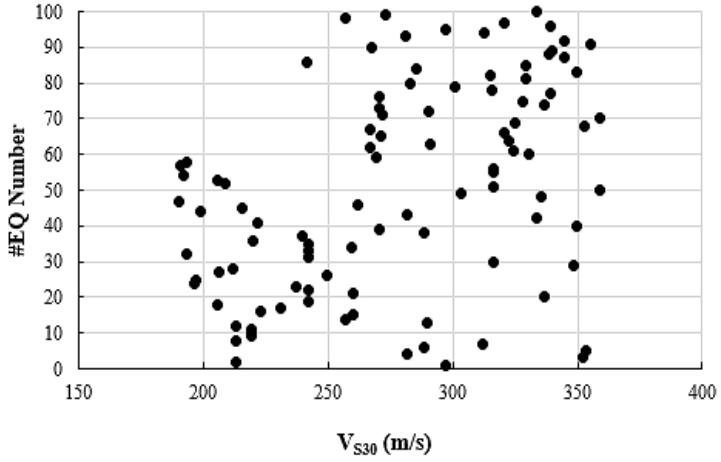

Figure 5: The average shear-wave velocities (V_{S30} values) in the top thirty meters of the soil for 100 selected earthquakes.

*Event Name (*3)*	*Station*	*Year*	M_w	I_A *(m/s)*	R_{JB} *(km)*	V_{S30} *(m/s)*	*PGA (g)*	*PGV (cm/s)*	*PGD (cm)*
Landers	Coolwater	1992	7.28	2.2	19.74	352.98	0.417	434.06	1524.82
Landers	Covina – W Badillo	1992	7.28	0.1	128.06	324.79	0.046	10.62	6.40
Landers	Desert Hot Springs	1992	7.28	0.7	21.78	359	0.154	20.87	7.77
Landers	Downey – Co Maint B.	1992	7.28	0.1	157.46	271.9	0.039	11.30	10.17
Landers	El Monte – Fair. Av	1992	7.28	0.1	135.88	290.63	0.038	11.81	16.12
Landers	Fountain Vall. – Euclid	1992	7.28	0.2	146.89	270.54	0.062	11.02	8.83
Landers	Hacienda Heights – C.	1992	7.28	0.1	136.29	337	0.049	8.44	4.71
Landers	Hemet Fire Station	1992	7.28	0.3	68.66	328.09	0.097	5.64	2.27
Landers	Huntington B.–Waikiki	1992	7.28	0.1	156	270.54	0.062	16.64	14.44
Landers	Indio – Coach. Canal	1992	7.28	0.3	54.25	339.02	0.109	15.11	9.79
Landers	Inglewood – Union Oil	1992	7.28	0.1	167.27	316.02	0.034	10.47	10.19
Landers	LA – 116th St School	1992	7.28	0.1	164.36	301	0.042	12.04	13.49
Landers	LA – E Vernon Ave	1992	7.28	0.1	157.69	283.14	0.041	16.20	16.34
Landers	LA – Fletcher Dr	1992	7.28	0.1	153.04	329.06	0.033	4.33	2.81
Landers	LA – N Westmoreland	1992	7.28	0.1	159.13	315.06	0.035	4.68	3.29
Landers	LA – Obregon Park	1992	7.28	0.1	151.7	349.43	0.065	7.66	5.59
Landers	LA – S Grand Ave	1992	7.28	0	161.56	285.28	0.047	17.07	21.09
Landers	LA – W 15th St	1992	7.28	0.1	160.99	329.52	0.038	12.63	15.04
Landers	LA – W 70th St	1992	7.28	0.1	163.96	241.41	0.051	14.76	12.84
Landers	LB – Orange Ave	1992	7.28	0.2	160.85	344.72	0.058	15.66	20.57
Landers	La Habra – Briarcliff	1992	7.28	0.1	143.12	338.27	0.047	11.52	8.94
Landers	La Puente – Rimg. Av	1992	7.28	0.1	132.08	339.52	0.043	9.83	4.90
Landers	Lakewood – Del A. B.	1992	7.28	0.2	157.41	267.35	0.051	15.50	14.67
Landers	Mission Creek Fault	1992	7.28	0.4	26.96	355.42	0.132	14.62	11.42
Landers	North Palm Springs	1992	7.28	0.7	26.84	344.67	0.134	14.53	5.70
Landers	Northridge–17645 Sat.	1992	7.28	0.1	172.32	280.86	0.040	16.72	16.46
Landers	Palm Springs Airport	1992	7.28	0.4	36.15	312.47	0.089	13.91	5.26
Landers	San Bern. – E & Hosp.	1992	7.28	0.4	79.76	296.97	0.087	14.57	7.63
Landers	Santa Fe Spr. – E.Joslin	1992	7.28	0.1	150.1	339.06	0.050	14.24	17.39
Landers	Sun Valley – Ros. B.	1992	7.28	0.1	163.54	320.93	0.028	8.41	5.20
Landers	Tarzana – Cedar Hill	1992	7.28	0.1	175.65	257.21	0.043	5.32	2.76
Parkfield-02, CA	Hollister–City Hall A.	2004	6.0	0	117.92	272.8	0.011	3.21	1.42
Parkfield-02, CA	Coalinga–Fire St. 39	2004	6.0	0.1	22.45	333.61	0.045	5.87	1.26

Table 3: Selected earthquake records [Part III: EQ 68-100], [46].

5 DETERMINATION OF ELASTIC EARTHQUAKE INPUT ENERGY SPECTRA USING SELECTED RECORDS

Input energy spectra of elastic SDOF systems having damping ratio of 5% were obtained using the selected real earthquakes. To that end, at first, the velocity-time histories ($\dot{u}(t)-t$) were computed by using the software PRISM [52]. Input energy-time histories ((E_I/m)-t

graphs) were then computed for the specific natural vibration period (T) of SDOF system. Period values were taken from T=0.1 sec. to T=3.0 sec. using the increment of ΔT=0.1 sec. For an accelerogram, 30 response time history (RTH) analyses were carried out. Totally, 3000 RTH analyses were performed and the maximum mass normalized earthquake input energy values ($(E_I/m)_{max}$) for all records were computed. The maximum energy-time histories for selected 100 earthquake records can be seen from Figure 8. Earthquakes were separated to 4 groups according to V_{S30} velocities (190 m/s<V_{S30}≤235 m/s, 235 m/s<V_{S30}≤280 m/s, 280 m/s<V_{S30}≤325 m/s and 325 m/s<V_{S30}≤370 m/s), and the input energy-time histories were computed for 4 earthquake groups (Figure 8). A computer algorithm was created in Excel by the author to combine the maximum input energies ($(E_I/m)_{max}$) and to obtain the input energy spectra. Velocity-time histories were taken from PRISM software [52].

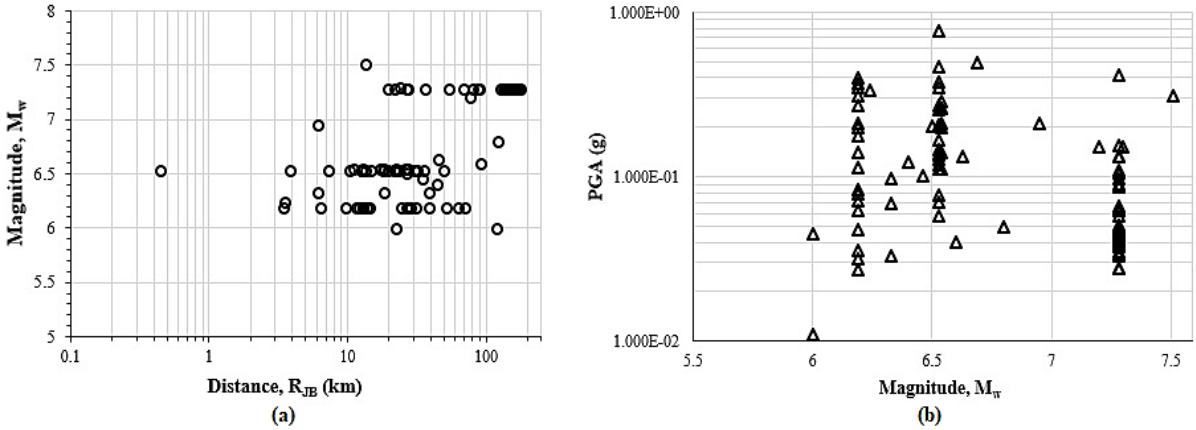

Figure 6: Strong motion data distribution of selected record set a) R_{JB} versus M_w scatter plots, b) M_w versus $PGA(g)$ scatter plots.

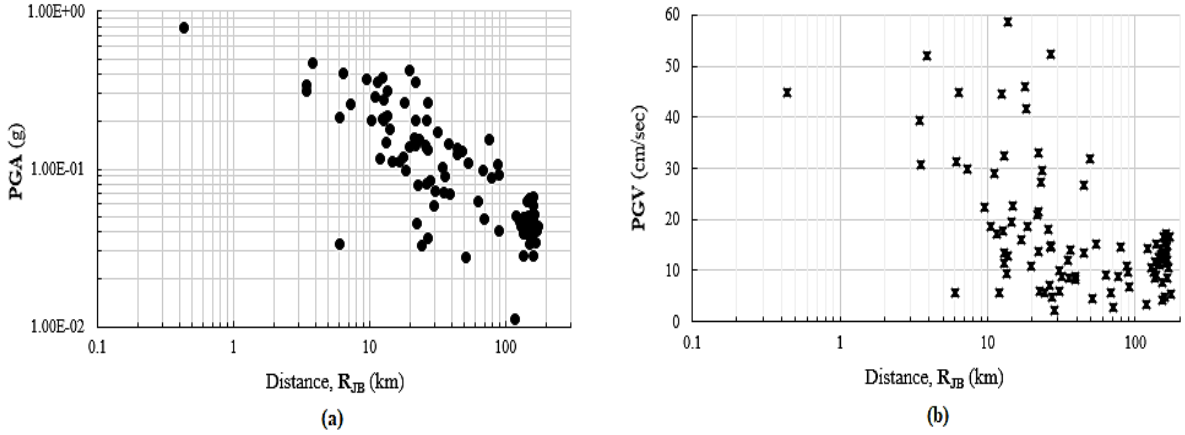

Figure 7: Distribution of strong motion data for distance R_{JB} a) in terms of PGA (g), b) in terms of PGV (cm/s).

The mass-normalized input energy spectra of elastic SDOF systems having 5% viscous damping ratio is shown in Figure 9. The energy spectra were created using the selected 100 earthquake records in Table 1, Table 2 and Table 3. The mean of input energy spectra and the mean+1 and +2 standard deviations were indicated in Figure 9 and also separately in Figure 10. From the variation coefficients (V_C) of elastic input energy spectra which are shown in Figure 10, it can be seen that the dispersion is generally considerable. Variation coefficients were also computed for 4 groups of earthquakes which were separated according to V_{S30} velocities (Figure 10).

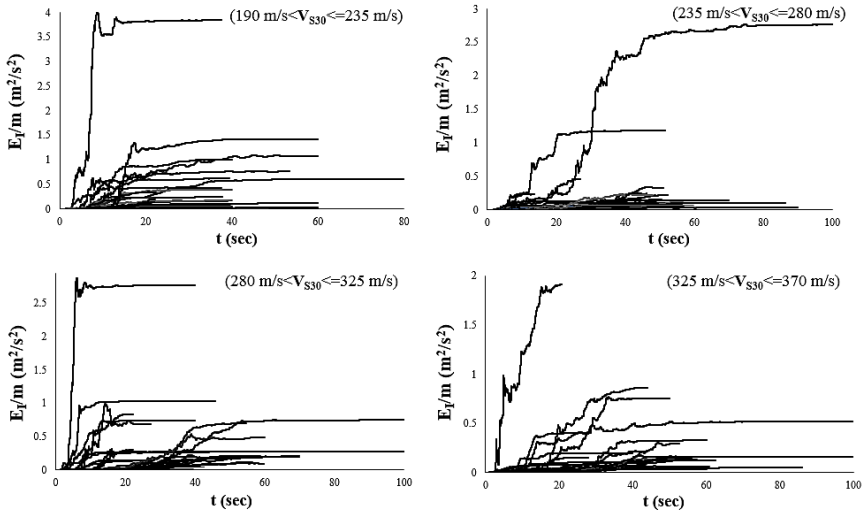

Figure 8: The maximum energy-time histories (E_I/m-t graphs) for selected 100 earthquake records (for 4 groups of V_{S30} velocities).

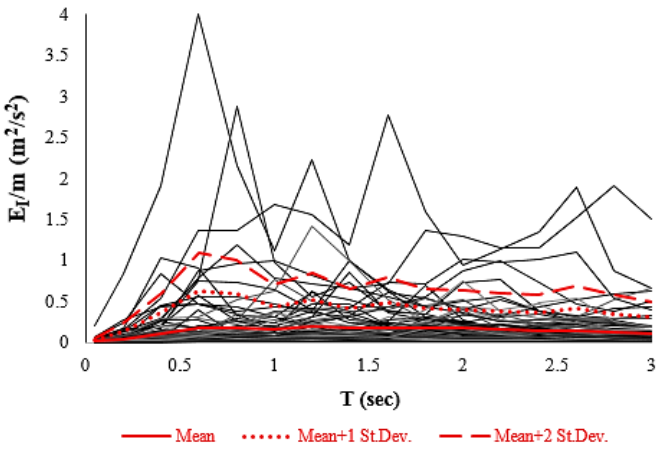

Figure 9: Mass-normalized elastic input energy spectra for Soil D and for 5% viscous damping ratio (E_I/m-T graphs), (with Mean, Mean+1 St.Dev. and Mean+2 St.Dev. of 100 selected ground motion records).

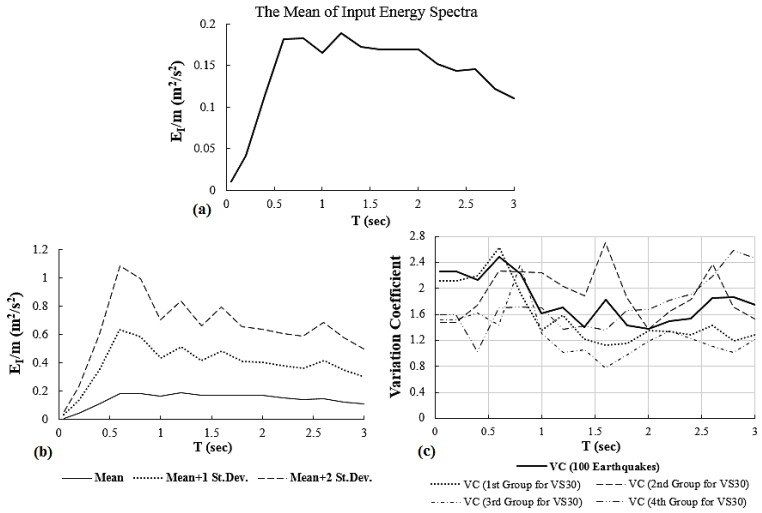

Figure 10: a) The mean of input energy spectra (The mean of 100 selected records), b) The input energy spectra graphs for: Mean, Mean+1 St.Dev. and Mean+2 St.Dev. values, c) Variation coefficients of the total selected records and variation coefficients of the separated 4 groups (according to V_{S30} velocities).

6 CLASSIFICATION OF EARTHQUAKE RECORDS ACCORDING TO V_{S30} VELOCITIES AND R_{JB} DISTANCES AND CREATING THE ELASTIC INPUT ENERGY SPECTRA OF DIFFERENT GROUPS

Earthquake records were classified according to V_{S30} velocities and R_{JB} distances within the study. Four ranges of V_{S30} were taken into account as: 190 m/s<V_{S30}≤235 m/s, 235 m/s<V_{S30}≤280 m/s, 280 m/s<V_{S30}≤325 m/s and 325 m/s<V_{S30}≤370 m/s, respectively. R_{JB} distances were separated to four groups as: 0 km<R_{JB}≤46 km, 46 km<R_{JB}≤92 km, 92 km<R_{JB}≤138 km and 138 km<R_{JB}≤184 km, respectively. V_{S30} and R_{JB} histograms may be shown in Figure 11. Number of records for V_{S30} and R_{JB} intervals can be obtained from Figure 11.

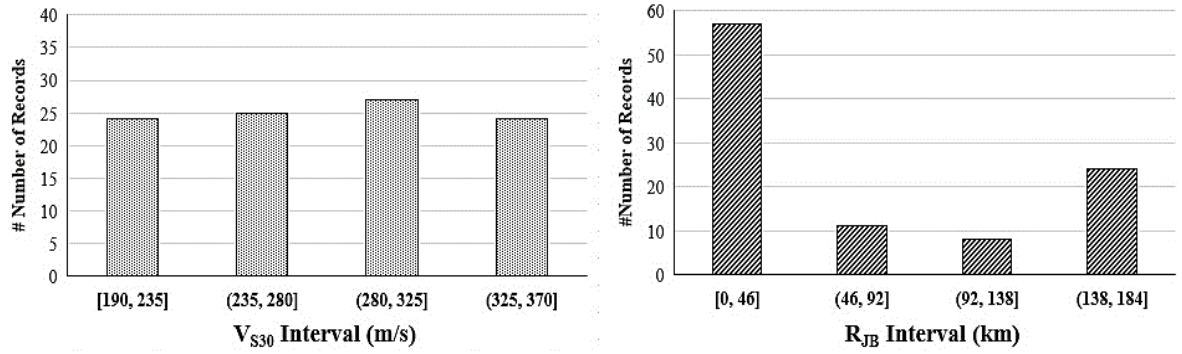

Figure 11: V_{S30} and R_{JB} histograms for selected earthquake records.

The elastic input energy spectra of earthquake groups according to V_{S30} velocities are shown in Figure 12. The mean of the spectra and the mean+1 and +2 standard deviations were indicated in the figure. With the increase in V_{S30} velocities, it was observed that the values of elastic input energy spectra tended to decrease gradually (Figure 12).

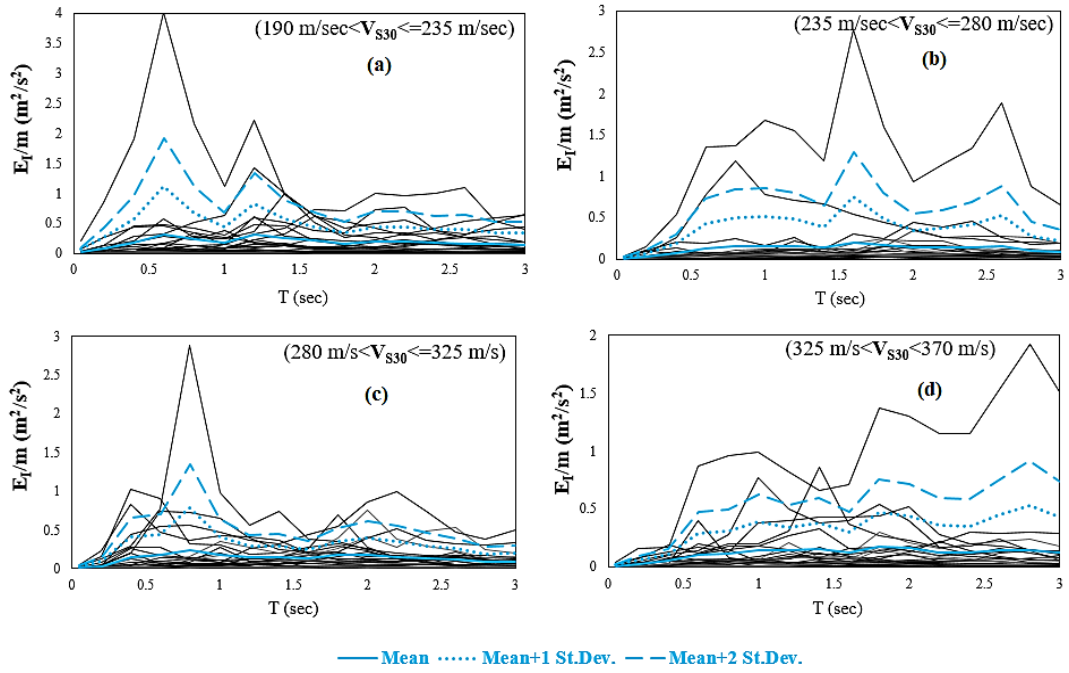

Figure 12: Mass-normalized input energy spectra of earthquakes: a) the group of V_{S30} between [190, 235] m/sec, b) the group of V_{S30} between (235, 280] m/sec, c) the group of V_{S30} between (280, 325] m/sec, d) the group of V_{S30} between (325, 370] m/sec.

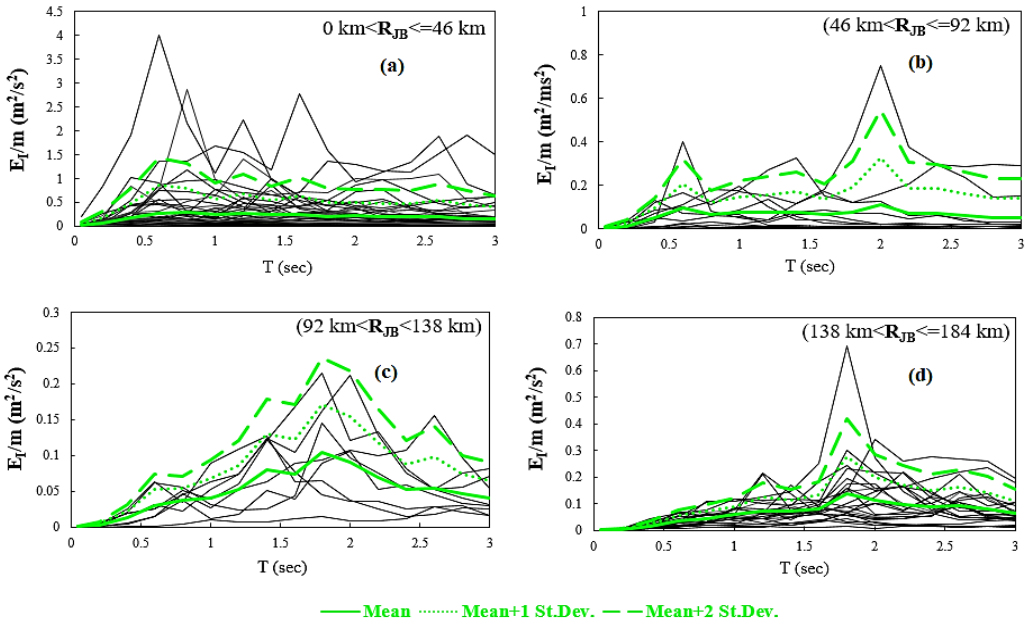

Figure 13: Mass-normalized input energy spectra of earthquakes: a) the group of R_{JB} between [0, 46] km, b) the group of R_{JB} between (46, 92] km, c) the group of R_{JB} between (92, 138] km, d) the group of R_{JB} between (138, 184] km.

The elastic input energy spectra of earthquake groups according to R_{JB} distances are shown in Figure 13. The mean of the spectra and the mean+1 and +2 standard deviations were indicated in the figure. With the increase in R_{JB} distances, it was observed that the values of elastic input energy spectra tended to decrease gradually (Figure 13). The maximum input energies were obtained for the interval of 0 km<R_{JB}≤46 km (Figure 13a).

7 ELASTIC DESIGN INPUT ENERGY SPECTRA FOR SELECTED EARTHQUAKES

Linear elastic design earthquake input energy spectrum was proposed for selected ground motions on site class D (on stiff soil with 180 m/s<V_{S30}≤360 m/s). The design energy demand spectrum was created for viscous damping ratio of 5% and the lower period was considered as T_0=0.05 sec. and the maximum period was considered as T_{max}=3.0 sec. The design spectral shapes were associated with simple mathematical expressions and smoothened curves as:

$$\begin{aligned} T_0 \le T \le T_1 \rightarrow \quad & \frac{E_I}{m} = a \cdot T + b \\ T_1 < T \le T_2 \rightarrow \quad & \frac{E_I}{m} = c \qquad \left(\frac{E_I}{m} \ in \ \frac{m^2}{s^2}\right) \\ T_2 < T \rightarrow \quad & \frac{E_I}{m} = k \cdot T^n \end{aligned} \tag{7}$$

where a, b, c, k and n are parameters of mass-normalized design input energy spectrum. Parameters depend on the soil type. In Equation (7); E_I/m is in unit of m^2/s^2. Parameter "a" represents the coefficient of period T in linear considered region of normalized spectrum and "b" is the constant parameter in region of T_0<T≤T_1. "c" is the maximum spectral value relative to the constant value of the spectrum. "n" is the exponential parameter governing the decrease in normalized spectrum for larger period values (T_2<T) and "k" is the multiplier of T_n (Figure 14).

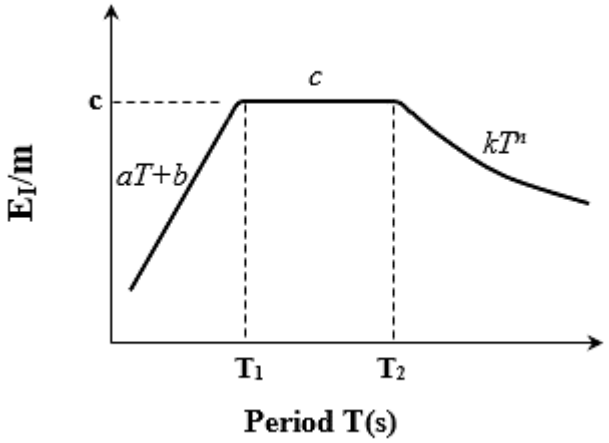

Figure 14: The spectral shape of elastic design input energy.

The fundamental design input energy spectrum shape is shown in Figure 14. T_1 is the period corresponding to the beginning of the constant value of the spectrum and T_2 is the period corresponding to the ending of the constant value of the spectrum (corner periods of the spectrum). Input energy spectra is the function of vibration period T, soil class and viscous damping ratio ξ [39]. ξ is assumed to be 5% in this study and the design input energy spectra were constructed for ξ=5%.

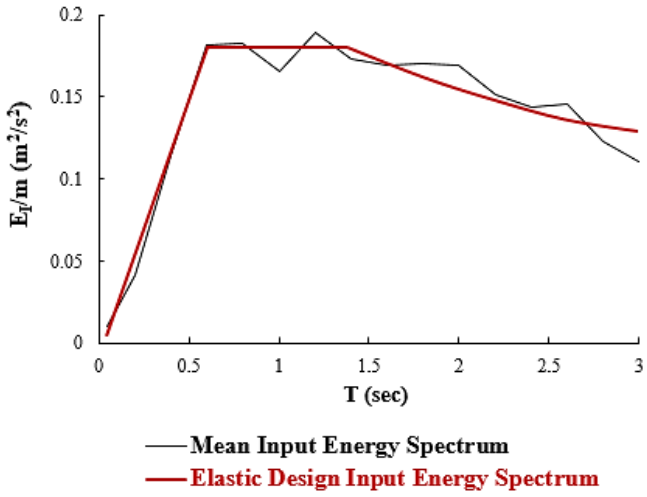

Figure 15: Elastic design input energy spectrum for selected 100 earthquake records on site class D and for ξ=5%.

The elastic design input energy spectrum for selected earthquakes within the study is shown in Figure 15. Statistical analyses were conducted and curve fitting which is the process of specifying the model that provides the best fit to the specific curves in the dataset was used. The results of linear regression analyses with *R*-squared values may be shown in Table 4 and Table 5. From Table 4; it can be concluded that the first region of the design spectrum ($T_0<T\leq T_1$ region) can be well-defined by linear model in Equation (7) ($a.T+b$). However, R-squared values showed that there is not a strong relation with data in the region of $T_2<T$ as there is in the first linear-considered region of the spectrum. It can be seen from Table 4 and Table 5 that the *R*-squared values are greater for "the mean of input energy spectrum".

$E_I/m - T$ (m^2/s^2)	a	b	T_1 (s)	R^2
Mean	0.3184	-0.0124	0.599	0.9918
Mean+1 St.Dev.	1.0982	-0.0529	0.597	0.9835
Mean+2 St.Dev.	1.878	-0.0934	0.601	0.9811

Table 4: Values of parameters introduced in Figure 14, for the elastic design input energy spectrum in Figure 15 (parameters for region of $T_0<T\leq T_1$).

$E_I/m - T$ (m^2/s^2)	c	T_2 (s)	k	n	R^2
Mean	0.1786	1.389	0.2508	-0.662	0.8371
Mean+1 St.Dev.	0.5423	1.198	0.5373	-0.420	0.7309
Mean+2 St.Dev.	0.9046	1.202	0.8575	-0.401	0.6579

Table 5: Values of parameters introduced in Figure 14, for the elastic design input energy spectrum in Figure 15 (parameters for region of $T_1<T\leq T_2$ and $T_2<T$).

The elastic design input energy spectra for earthquake groups which were separated according to V_{S30} velocities and R_{JB} distances (see intervals in histograms of Figure 11) are shown in Figure 16. Parameters of design input energy spectra (a, b, c, k, n, T_1 and T_2) are presented by Table 6, Table 7, Table 8 and Table 9. In the group with lower V_{S30} velocities (especially the group: 190 m/s$<V_{S30}\leq$235 m/s), the design input energy spectrum was obtained greater for SDOF systems having damping ratio of 5%. The design input energy spectrum was obtained greater for the earthquake group having R_{JB} distances between 0 km$<R_{JB}\leq$46 km. The elastic design input energy spectra of different groups were shown by different colors. All design energy spectra in Figure 16 were created considering the mean of input energy spectra of different groups (from the mean spectra in Figure 12 and Figure 13).

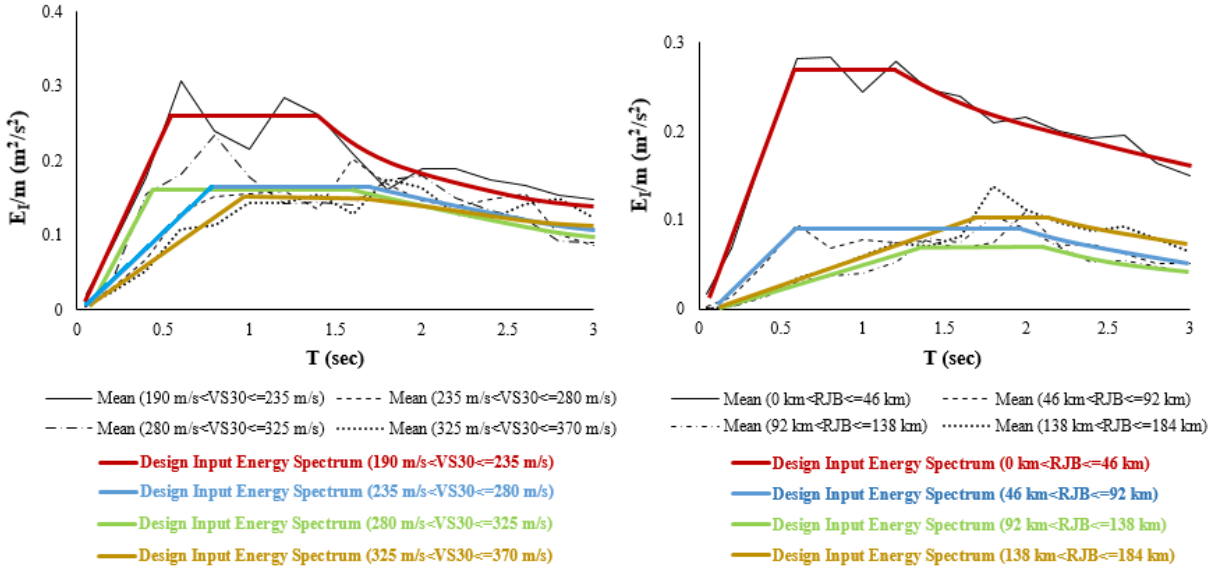

Figure 16: Elastic design input energy spectra for earthquake groups (in Figure 11) according to V_{S30} velocities and R_{JB} distances (for ξ=5%).

Design $E_I/m - T$ (m^2/s^2)	a	b	T_1 (s)	R^2
$190\ m/s<V_{S30}<=235\ m/s$	0.5179	-0.0152	0.512	0.9905
$235\ m/s<V_{S30}<=280\ m/s$	0.2080	-0.0083	0.761	0.9778
$280\ m/s<V_{S30}<=325\ m/s$	0.4295	-0.0258	0.485	0.9316
$325\ m/s<V_{S30}<=370\ m/s$	0.1500	-0.0022	0.975	0.9662

Table 6: Values of parameters introduced in Figure 14, for the elastic design input energy spectrum of different V_{S30} groups (parameters for region of $T_0<T\leq T_1$).

Design $E_I/m - T$ (m^2/s^2)	c	T_2 (s)	k	n	R^2
$190\ m/s<V_{S30}<=235\ m/s$	0.2662	1.389	0.2825	-0.587	0.7271
$235\ m/s<V_{S30}<=280\ m/s$	0.1598	1.720	0.3335	-1.079	0.7527
$280\ m/s<V_{S30}<=325\ m/s$	0.1578	1.709	0.4658	-1.479	0.9177
$325\ m/s<V_{S30}<=370\ m/s$	0.1475	1.715	0.2215	-0.505	0.5167

Table 7: Values of parameters introduced in Figure 14, for the elastic design input energy spectrum of different V_{S30} groups (parameters for region of $T_1<T\leq T_2$ and $T_2<T$).

Design $E_I/m - T$ (m^2/s^2)	a	b	T_1 (s)	R^2
$0\ km<R_{JB}<=46\ km$	0.4914	-0.0165	0.585	0.9937
$46\ km<R_{JB}<=92\ km$	0.1718	-0.0126	0.594	0.9691
$92\ km<R_{JB}<=138\ km$	0.0544	-0.0060	1.405	0.9525
$138\ km<R_{JB}<=184\ km$	0.0672	-0.0083	1.697	0.9246

Table 8: Values of parameters introduced in Figure 14, for the elastic design input energy spectrum of different R_{JB} groups (parameters for region of $T_0<T\leq T1$).

Design $E_I/m - T$ (m^2/s^2)	c	T_2 (s)	k	n	R^2
$0\ km<R_{JB}<=46\ km$	0.2681	1.198	0.3101	-0.581	0.9212
$46\ km<R_{JB}<=92\ km$	0.090	1.980	0.2173	-1.340	0.8915
$92\ km<R_{JB}<=138\ km$	0.080	2.150	0.2279	-1.547	0.9142
$138\ km<R_{JB}<=184\ km$	0.108	2.155	0.2498	-1.149	0.8640

Table 9: Values of parameters introduced in Figure 14, for the elastic design input energy spectrum of different R_{JB} groups (parameters for region of $T_1<T\leq T_2$ and $T_2<T$).

8 CONCLUSIONS

This paper presents the development of elastic design input energy spectra using real ground motion records. The effect of the average shear-wave velocity in the top thirty meters of the soil (V_{S30}) and the effect of the Joyner-Boore distance (R_{JB}) on the elastic input energy spectra are also investigated. Actual ground motion records taken from many different earthquakes all over the world are selected to investigate the elastic input energy spectra for damping ratio of 5%. Selected ground motions are all on the same site class according to National Earthquake Hazards Reduction Program site classification. Elastic input energy spectra of the selected ground motions are computed and the proposal of design input energy spectra are carried out. The study mainly focuses on the development of elastic design input energy spectra of real ground motions on stiff soil. Ground motion records are separated into four groups considering the V_{S30} velocities and R_{JB} distances and the design input energy spectra of each group are also investigated independently. The design spectral shapes are expressed with simple mathematical expressions and idealized lines and curves. Coefficient of determination values are computed for each region of the design spectra to measure of how close the data are to the fitted regression lines. The effect of the change in V_{S30} velocities and R_{JB} distances on the elastic design input energy spectra of real earthquakes is investigated. The results of the study are restricted to the selected ground motions which are on stiff soil with 180 m/s$<V_{S30}\leq$360 m/s. The notable findings of the study are as follows:

- The mean input energy spectrum of selected earthquakes has a very good correlation with the proposed design elastic input energy spectra. Coefficient of determination (R-squared) value for the first region of the design input energy spectrum (for $T_0<T\leq T_1$ region) is obtained as 0.9918 so, the region can be well-defined by linear model. For larger period values (for $T_2<T$), the coefficient of determination (R-squared) value is obtained as 0.8371. The region can also be well-defined with the curve $k.T_n$. However, the linear regression in $T_0<T\leq T_1$ region shows that there is stronger correlation between the real input energy spectra and the proposed design input energy spectra in that region than the region of $T_2<T$.

- The type of soil (so V_{S30} velocity) has a significant influence on the design input energy spectra. Elastic input energy spectra decrease as V_{S30} velocity increases (from soft soil to stiff soil). However, the decrease is obtained more significant from the first selected earthquake group to the second selected earthquake group (from the group having 190 m/s$<V_{S30}\leq$235 m/s to the group having 235 m/s$<V_{S30}\leq$280 m/s). The results of the study are valid for selected earthquake records.

- Elastic input energy spectra are obtained maximum for the earthquake group with 0 km$<R_{JB}\leq$46 km. It can be seen from the study that the input energy spectra tend to decrease with the increase in R_{JB} distance. As the shortest distance from a site to the surface projection of the rupture surface (R_{JB}) becomes very smaller, the values of elastic input energy spectra becomes higher.

- In the 3rd earthquake group having 280 m/s$<V_{S30}\leq$325 m/s, the coefficient of variation for the elastic input energy spectra is obtained smaller when it is compared to other groups. The input energy spectra of this group scattered around the mean spectra better than other earthquake groups.

- It is observed from the study that the elastic input energy spectra of near fault earthquakes are higher than that of the far fault records. The records which have the source-to-site distance is less than 15 km show an instantaneous jump in the input energy spectrum graph. If the near fault earthquakes were extracted from the selected earthquakes within the study, the proposed design input energy spectra graph could be smoother and lower.

The elastic design input energy spectra may be used in seismic design of structures if the energy capacity of structures can be determined. The main purpose of this study is to propose demand design energy spectra for selected earthquakes. Further studies can be done using wide range of ground motion records which are on different soil sites. The study can be extended for SDOF systems having different damping ratios. Inelastic SDOF systems having different ductility ratios can be analyzed to obtain the inelastic input energy spectra. Different cyclic models can be used to define the nonlinear force-displacement relation. It should be noted that each earthquake reflects its own characteristics in dynamic analyses and in seismic input energy computations.

REFERENCES

[1] International Conference of Building Officials (ICBO), UBC-97: *Uniform Building Code*. Whittier, CA, 1997.

[2] European Committee for Standardization (CEN), Eurocode 8: *Design of Structures for Earthquake Resistance*. B-1050 Brussels, 2004.

[3] National Research Council of Canada, *National Building Code of Canada* (NBCC 2005). Ottawa, NRCC 47666, 2005.

[4] International Code Council (ICC), *International Building Code* (IBC 2006). Country Club Hills, Illinois, 2006.

[5] Ministry of Public Works and Settlement, *Turkish Seismic Design Code* (TSDC 2007). Ankara, Turkey, 2007.

[6] American Society of Civil Engineers (ASCE), ASCE/SEI Standard 7-10: *Minimum Design Loads for Buildings and Other Structures*. Virginia, 2010.

[7] The Disaster and Emergency Management Authority, *Turkish Building Earthquake Code*. Published in Official Gazette on 18th of March, Ankara, Turkey, 2018.

[8] M.J.N. Priestley, M.C. Calvi, M.J. Kowalsky, *Displacement-based seismic design of structures*. Pavia: IUSS Press, 2007.

[9] J.J. Bommer, A.S. Elnashai, Displacement spectra for seismic design. *Journal of Earthquake Engineering*, **3**(1), 1-32, 1999.

[10] M.J.N. Priestley, Myths and fallacies in earthquake engineering – conflicts between design and reality. *Bulletin of the New Zealand Society for Earthquake Engineering*, **26**(3), 329-341, 1993.

[11] G.M. Calvi, M.J.N. Priestley, M.J. Kowalsky, Displacement–based seismic design of structures. *3rd National Conference on Earthquake Engineering and Engineering Seismology*, Athens, Greece, 2008.

[12] M.J.N. Priestley, M.J. Kowalsky, Direct displacement–based seismic design of concrete building. *Bulletin of the New Zealand Society for Earthquake Engineering*, **33**(4), 421-444, 2000.

[13] N.A. Karimzada, E. Aktas, Performance–based seismic design of reinforced concrete frame buildings: a direct displacement–based approach. *12th International Congress on Advances in Civil Engineering*, Bogazici University, Istanbul, Turkey, 2016.

[14] S.A. Freeman, J.P. Nicoletti, J.V. Tyrell, Evaluation of existing buildings for seismic risk – a case study of Puget sound naval shipyard. *First U.S. Conference on Earthquake Engineering*, Bremerton, Washington, 1975.

[15] Prestandard and Commentary for The Seismic Rehabilitation of Buildings, *FEMA 356*. Washington DC., 2000.

[16] Applied Technology Council, FEMA 440: *Improvement of Nonlinear Static Seismic Analysis Procedures*. Washington DC., 2005.

[17] American Society of Civil Engineers (ASCE), ASCE/SEI Standard 41-06: *Seismic Rehabilitation and Evaluation of Existing Buildings*. Reston, VA, 2007.

[18] G.G. Amiri, F.M. Dana, S. Sedighi, Determination of design acceleration spectra for different site conditions, magnitudes, safety levels and damping ratios in Iran. *International Journal of Civil Engineering*, **6**(3), 2008.

[19] C.M. Uang, V.V. Bertero, Evaluation of seismic energy in structures. *Earthquake Engineering & Structural Dynamics*, **19**(1), 77-90, 1990.

[20] V.V. Bertero, A. Teran-Gilmore, Use of energy concepts in earthquake resistant analysis and design: issues and future directions. *Advances in Earthquake Engineering Practice*, Short Course in Structural Engineering, Architectural and Economic Issues, University of California, Berkeley, 1994.

[21] B. Akbas, J. Shen, Earthquake-resistant design (EQRD) and energy concepts (in Turkish). *Technical Journal of Turkish Chamber of Civil Engineers*, Article 192, 2877–2901, 2003.

[22] G.W. Housner, Limit design of structures to resist earthquakes. *Proceedings of the First World Conference on Earthquake Engineering*, Oakland, California, USA, 186–198, 1956.

[23] P. Fajfar, M.A. Fischinger, Seismic procedure including energy concept. *Ninth European Conference on Earthquake Engineering (ECEE)*, **2**, 312-321, Moscow, 1990.

[24] G. Manfredi, Evaluation of seismic energy demand. *Earthquake Engineering & Structural Dynamics*, **30**(4), 485-499, 2001.

[25] T.F. Zahrah, W.J. Hall, Earthquake energy absorption in SDOF structures. *Journal of Structural Engineering*, **110**(8), 1757-1772, 1984.

[26] H. Akiyama, *Earthquake-resistant limit-state design for buildings*. University of Tokyo Press, Japan, 1985.

[27] H. Kuwamura, T.V. Galambos, Earthquake load for structural reliability. *Journal of Structural Engineering*, **115**(6), 1446-1462, 1989.

[28] P. Fajfar, T. Vidic, M. Fischinger, *Seismic demand in medium- and long-period structures. Earthquake Engineering & Structural Dynamics*, **18**(8), 1133-1144, 1989.

[29] B. Akbas, J. Shen, H. Hao, Energy approach in performance-based seismic design of steel moment resisting frames for basic safety objective. *The Structural Design of Tall and Special Buildings*, **10**(3), 193-217, 2001.

[30] B. Akbas, J. Shen, Energy approach in performance-based earthquake resistant design (PB-EQRD). *Proceedings of the 12th European Conference on Earthquake Engineering*, London, UK, Paper No. 043, 2002.

[31] B. Akbas, J. Shen, A.N. Cetiner, Energy approach in performance-based earthquake resistant design and determining the reliability of SDOF systems using energy concepts. Research Fund Report, Department of Earthquake and Structural Science, Gebze Institute of Technology, No: Ol-B-02-01-15, 2002.

[32] S. Leelataviwat, S.C. Goel, B. Stojadinovic, Energy-based seismic design of structures using yield mechanism and target drift. *Journal of Structural Engineering*, **128**(8), 1046-1054, 2002.

[33] S. Leelataviwat, W. Saewon, S.C. Goel, An energy-based method for seismic evaluation of structures. *Proceedings of the 14th World Conference on Earthquake Engineering*: Innovation Practice Safety, Bejing, China, 2008.

[34] S. Leelataviwat, W. Saewon, S.C. Goel, Application of energy balance concept in seismic evaluation of structures. *Journal of Structural Engineering*, **135**(2), 113-121, 2009.

[35] S. Terapathana, *An energy method for earthquake resistant design of RC structures*. PhD Thesis, University of Southern California, Los Angeles, CA, USA, 2012.

[36] S.A. Enderami, S.B. Beheshti-Aval, M.A. Saadeghvaziri, New energy based approach to predict seismic demands of steel moment resisting frames subjected to near-fault ground motions. *Engineering Structures*, **72**, 182-192, 2014.

[37] P. Fajfar, T. Vidic, Consistent inelastic design spectra: hysteretic and input energy. *Earthquake Engineering & Structural Dynamics*, **23**, 523-537, 1994.

[38] H. Sucuoglu, A. Nurtug, Earthquake ground motion characteristics and seismic energy dissipation. *Earthquake Engineering & Structural Dynamics*, **24**, 1195-1213, 1995.

[39] L.D. Decanini, F. Mollaioli, Formulation of elastic earthquake input energy spectra. *Earthquake Engineering & Structural Dynamics*, **27**, 1503-1522, 1998.

[40] A. Benavent-Climent, L.G. Pujades, F. López-Almansa, Design energy input spectra for moderate seismicity regions. *Earthquake Engineering & Structural Dynamics*, **31**, 1151-1172, 2002.

[41] F. López-Almansa, A.U. Yazgan, A. Benavent-Climent, Design energy input spectra for high seismicity regions based on Turkish registers. *Bulletin of Earthquake Engineering*, **11**(4), 885-912, 2013.

[42] A.A. Dindar, C. Yalcin, E. Yuksel, H. Ozkaynak, O. Buyukozturk, Development of earthquake energy demand spectra. *Earthquake Spectra*, **31**(3), 1667-1689, 2015.

[43] P. Quinde, E. Reinoso, A. Terán-Gilmore, Inelastic seismic energy spectra for soft soils: application to Mexico City. *Soil Dynamics and Earthquake Engineering*, **89**, 198-207, 2016.

[44] F.S. Alici, H. Sucuoglu, Prediction of input energy spectrum: attenuation models and velocity spectrum scaling. *The Fourth International Conference on Earthquake Engineering and Seismology*, 11-13 October, Anadolu University, Eskisehir, Turkey, 2017.

[45] V. Ozsarac, S. Karimzadeh, M.A. Erberik, A. Askan, Energy-based response of simple structural systems by using simulated ground motions. *Procedia Engineering*, **199**, 236-241, 2017.

[46] Pacific Earthquake Engineering Research (PEER) Center. PEER Ground Motion Database, available at https://ngawest2.berkeley.edu (last accessed 2 May 2018).

[47] Building Seismic Safety Council (BSSC), *National Earthquake Hazards Reduction Program Recommended Seismic Provisions for New Buildings and Other Structures*, Part 1: Provisions, Federal Emergency Management Agency (FEMA P-750), Washington, D.C., 2009.

[48] Y.M. Fahjan, Selection and scaling of real earthquake accelerograms to fit the Turkish design spectra. *Technical Journal of Turkish Chamber of Civil Engineers, Digest 2008*, 1231-1250, 2008.

[49] B.Ö. Ay, S. Akkar, A procedure on ground motion selection and scaling for nonlinear response of simple structural systems. *Earthquake Engineering & Structural Dynamics* **41**, 1693-1707, 2012.

[50] E. Kalkan, A. Chopra, *Practical guidelines to select and scale earthquake records for nonlinear response history analysis of structures*. Earthquake Engineering Research Institute (EERI), Open File Report, 2010.

[51] A. Arias, *A measure of earthquake intensity in seismic design for nuclear power plants*. MIT Press, Cambridge, Massachusetts, 438-483, 1970.

[52] PRISM for Earthquake Engineering, *A software for seismic response analysis of single-degree-of freedom systems*. Department of Architectural Engineering, INHA University, 2010.